

1

Introduction

My little machine was a primitive precursor of this type of accelerator which today is called a 'linac' for short. However, I must now emphasize one important detail. The drift tube was the first accelerating system which had earthed potential on both sides, i.e. at both the particles' entry and exit, and was still able to accelerate the particles exactly as if a strong electric field was present. This fact is not trivial. In all naiveté one may well expect that, when the voltage on the drift tube was reversed, the particles flying within would be decelerated, which is clearly not the case. After I had proven that such structures, earthed at both ends, were effectively possible, many other such systems were invented. – Rolf Wideröe

[From *The Infancy of Particle Accelerators*, edited by Pedro Waloschek, see ref. [4]]

During the second half of the twentieth century, the linear accelerator has undergone a remarkable development. Its technological base is a consequence of the science of both the nineteenth and twentieth centuries, including the discoveries of electromagnetism by Faraday, Maxwell, and Hertz in the nineteenth century and the discovery of superconductivity in the twentieth century. The design of a linear accelerator requires an understanding of the major areas of classical physics, especially classical mechanics, and electromagnetism, as well as relativity theory. The linear accelerator has developed as a great tool for learning about the world of subatomic particles. The linear accelerator provides beams of high quality and high energy, sufficient to resolve the internal structure of the nucleus and of its constituent subnuclear particles. Like a microscope, it has probed the internal structure of the atomic nucleus and of the nuclear constituents, the proton and neutron. Measurements made using the beams from an electron linear accelerator have given us our present picture of the proton, that it is made of pointlike particles called *quarks*. Furthermore, the linear accelerator has been applied in hospitals throughout the world as a source of X rays for radiation therapy to treat cancer. This application may represent the most significant spin-off of high-energy and nuclear physics research for the benefit of mankind. The linear accelerator is truly one of the most significant examples of high-technological development in the postindustrial era. The sizes of linacs range from a few meters to a few kilometers, and the costs range from a few million to a billion dollars, depending on the final energy.

As a research tool alone, we can expect that the linear accelerator will have a great future in the twenty-first century. The straight-line trajectory avoids power losses caused by synchrotron radiation that accompanies circular radio frequency (RF) accelerators. The capability for providing strong focusing allows high-quality and high-intensity beams that enable precision measurements to be made, and provides high-power beams for many applications. We can anticipate continuing progress in areas such as radio-frequency quadrupole (RFQ) linacs, colliding beams, high-power beams, high-frequency RF power and microwave technology, and RF superconductivity. Further developments in these areas will lead the linac to new performance levels with higher currents, better beam quality, and lower power requirements. We can confidently expect an expansion to new applications in the medical and industrial areas. The purpose of this book is to present the scientific and technical foundations of the linear accelerator, how it works, and why it will continue to serve as a powerful tool for the study of nature, and for many other practical applications.

1.1 Linear Accelerators: Historical Perspective

It might be expected that the term *linear accelerator* should refer to any device in which particles are accelerated along a straight line. However, through common usage in the accelerator field the term *linear accelerator* has been reserved for an accelerator in which charged particles move on a linear path, and are accelerated by time-dependent electromagnetic fields. The abbreviation *linac* is commonly used for the term *linear accelerator*. In a RF linac, the beam is accelerated by RF electromagnetic fields with a harmonic time dependence [1]. The first formal proposal and experimental test for a linac was by Rolf Wideröe in 1928, but linear accelerators that were useful for research in nuclear and elementary particle research did not appear until after the developments of microwave technology in World War II, stimulated by radar programs. Since then, the progress has been rapid, and today, the linac is not only a useful research tool, but is also being developed for many other important applications.

A particle accelerator delivers energy to a charged-particle beam by application of an electric field. The first particle accelerators were electrostatic accelerators in which the beam gains energy from a constant electric field. Each particle acquires an energy equal to the product of its electric charge times the potential drop, and the use of electrostatic fields led to a unit of energy called the electron volt (eV), equal to the product of the charge times the voltage drop. The main limitation of electrostatic accelerators is that the maximum energy obtainable cannot exceed the product of the charge times the potential difference that can be maintained, and in practice this potential difference is limited by electric breakdown to no more than a few tens of megavolts. RF accelerators bypass this limitation by applying a harmonic

time-varying electric field to the beam, which is localized into bunches, such that the bunches always arrive when the field has the correct polarity for acceleration. The time variation of the field removes the restriction that the energy gain be limited by a fixed potential drop. The beam is accelerated within electromagnetic-cavity structures, in which a particular electromagnetic mode is excited from a high-frequency external power source. For acceleration, the beam particles must be properly phased with respect to the fields, and for sustained energy gain they must maintain synchronism with those fields. The latter requirement has led to the name *resonance accelerators*, which includes the linac, cyclotron, and synchrotron. The ideal particle orbit in an RF accelerator may be either a straight line for a linac, a spiral for a cyclotron, or a circle for a synchrotron.

In 1924, Gustav Ising of Stockholm proposed the first accelerator that used time-dependent fields, consisting of a straight vacuum tube, and a sequence of metallic drift tubes with holes for the beam [2]. The particles were to be accelerated from the pulsed voltages that were generated by a spark discharge and applied across adjacent drift tubes. Synchronism of the applied voltage pulses with the beam particles was to be obtained by introducing transmission lines, chosen to delay the pulse from the voltage source to each of the drift tubes. The concept proposed by Ising was not tested at that time, but the publication was very important because it influenced the young Norwegian student, Rolf Wideröe.

The first RF linear accelerator was conceived and demonstrated experimentally by Wideröe in 1927 at Aachen, Germany. It was reported in a paper [3] that is one of the most significant in the history of particle accelerators,[4] and which inspired E. O. Lawrence to the invention of the cyclotron [5]. The linac built by Wideröe was the forerunner of all modern RF accelerators. The Wideröe linac concept, shown in Fig. 1.1, was to apply a time-alternating voltage to a sequence of drift tubes, whose lengths increased with increasing particle velocity, so that the particles would arrive in every gap at the right time to be accelerated. In the figure, D are drift tubes connected to an alternating voltage source V that applies equal and opposite voltages to sequential drift tubes, G are the gaps between the drift tubes in which the electric force acts to accelerate the particles, and S is the source of a continuous ion beam. For efficient acceleration the particles must be grouped into bunches (shown by

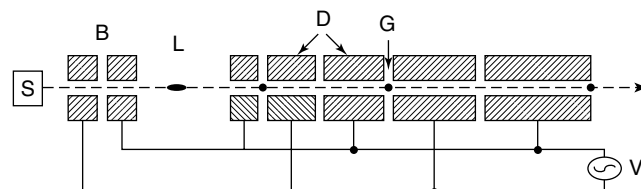


Figure 1.1 Concept of the Wideröe drift-tube linac.

the black dots), which are injected into the linac at the time when the polarity of the drift tubes is correct for acceleration. The bunching can be accomplished by using an RF gap B between the dc source and the linac. This gap impresses a velocity modulation on the incoming beam that produces spatial bunching at the end of a suitable drift space L. The net effect of the sequence of voltage kicks is to deliver a total voltage gain to the beam, which is greater than the impressed voltage V in any single gap.

In Wideröe's experiment, an RF voltage of 25 kV from a 1-MHz oscillator was applied to a single drift tube between two grounded electrodes, and a beam of singly charged potassium ions gained the maximum energy in each gap. A final beam energy of 50 keV was measured, which is twice that obtainable from a single application of the applied voltage. This was also the first accelerator that had ground potential at both the entrance and the exit ends, and was still able to deliver a net energy gain to the beam, using the electric fields within. The experiment established the principle that, unlike an electrostatic accelerator, the voltage gain of an RF accelerator could exceed the maximum applied voltage. There was no reason to doubt that the method could be repeated as often as desired to obtain unlimited higher energies. In 1931 Sloan and Lawrence [6] built a Wideröe-type linac with 30 drift tubes, and by applying 42 kV at a frequency of 10 MHz, they accelerated mercury ions to an energy of 1.26 MeV at a beam current of 1 μ A. By 1934 the output energy had been raised to 2.85 MeV [7] using 36 drift tubes.

The original Wideröe linac concept was not suitable for acceleration to high energies of beams of lighter protons and electrons, which was of greater interest for fundamental physics research. These beam velocities are much larger, approaching the speed of light, and the drift-tube lengths and distances between accelerating gaps would be impractically large, resulting in very small acceleration rates, unless the frequency could be increased to near a gigahertz. In this frequency range, the wavelengths are comparable to the ac circuit dimensions, and electromagnetic-wave propagation and electromagnetic radiation effects must be included for a practical accelerator system. For example, for an electron linac the lengths of the drift tubes and supporting stems would equal nearly a half a wavelength, and instead of isopotential electrodes they would function more like resonant antennas with high power losses. Thus, linac development required higher-power microwave generators, and accelerating structures better adapted for high frequencies and for acceleration requirements of high-velocity beams. High-frequency power generators, developed for radar applications, became available after World War II. At this time, a new and more efficient high-frequency proton-accelerating structure, based on a linear array of drift tubes enclosed in a high-Q cylindrical cavity, was proposed by Luis Alvarez [8] and coworkers at the University of California. The drift-tube linac (DTL) concept was to excite a mode with a uniform electric field in the gaps and zero field inside the drift tubes to avoid deceleration when the field was reversed. A 1-m diameter, 12-m DTL with a resonant frequency of 200 MHz was built,[9] which accelerated

protons from 4 to 32 MeV. At about the same time at Stanford a new, efficient accelerating structure for relativistic electrons was proposed, consisting of an array of pillbox-cavity resonators with a central hole in each end wall for propagation of both the beam and the electromagnetic energy. The structure was called the *disk-loaded* or *iris-loaded waveguide*, [10] and this development led eventually to the 3-km Stanford Linear Accelerating Center (SLAC) linac. From these two projects the first modern proton and electron linacs were born. [11]

The RF linear accelerator is classified as a resonance accelerator. Because both ends of the structure are grounded, a linac can easily be constructed as a modular array of accelerating structures. The modern linac typically consists of sections of specially designed waveguides or high-Q resonant cavities that are excited by RF electromagnetic fields, usually in the VHF and UHF microwave frequency ranges. The accelerating structures are tuned to resonance and are driven by external, high-power RF-power tubes, such as klystrons, or various types of gridded vacuum tubes. The ac (wall plug) to RF efficiencies of these tubes typically range from about 40 to 60%. The output electromagnetic energy from the tubes is transported in conventional transmission lines or waveguides to the linac structure. The accelerating structures must efficiently transfer the electromagnetic energy to the beam, and this is accomplished in two important ways. First, the resonant buildup of the fields in the high-Q structure transforms the low field levels of the input waveguide into high fields within the structure and produces a large ratio of stored electromagnetic energy relative to the ohmic energy dissipated per cycle. Second, through an optimized configuration of the internal geometry, the structure can concentrate the electric field along the trajectory of the beam promoting maximal energy transfer. The most useful figure of merit for high field concentration on the beam axis and low ohmic power loss is the shunt impedance.

One of the main advantages of the linear accelerator is its capability for producing high-energy, and high-intensity charged-particle beams of high beam quality, where high beam quality can be related to a capacity for producing a small beam diameter and small energy spread. Other attractive characteristics of the linac include the following: (1) strong focusing can be easily provided to confine a high-intensity beam; (2) the beam traverses the structure in a single pass, and therefore repetitive error conditions causing destructive beam resonances are avoided; (3) because the beam travels in a straight line, there is no power loss from synchrotron radiation, which is a limitation for high-energy electron beams in circular accelerators; (4) injection and extraction are simpler than in circular accelerators, since the natural orbit of the linac is open at each end; special techniques for efficient beam injection and extraction are unnecessary; (5) the linac can operate at any duty factor, all the way to 100% duty or a continuous wave (CW), which results in acceleration of beams with high average current.

1.2

Linac Structures

A simplified block diagram of a linac in Fig. 1.2 shows a linac structure with accelerating cavities and focusing magnets, and supplied with electromagnetic energy by an RF-power system. Beam is injected from a dc injector system. A vacuum system is required for good beam transmission. Electric power is used primarily by the RF-power system. A cooling system (water for normal-conducting linacs and liquid helium for superconducting linacs) removes the heat generated by the resistive wall losses. Because the linac uses a sinusoidally varying electric field for acceleration, particles can either gain or lose energy depending on the beam phase relative to the crest of the wave. To provide efficient acceleration for all the particles, the beam must be bunched as shown in Fig. 1.3. The bunches may be separated longitudinally by one or more RF periods.

Figure 1.4 shows the electric- and magnetic-field patterns in a simple cylindrical cavity operated in a transverse-magnetic resonant mode. Such a

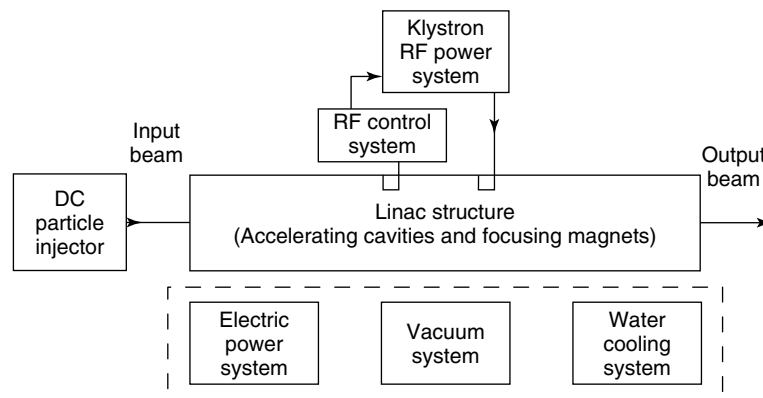


Figure 1.2 Simplified block diagram of a linac.

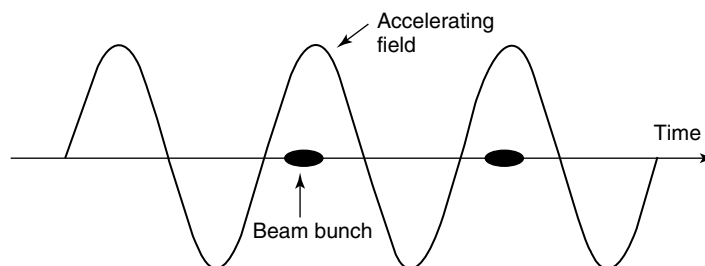


Figure 1.3 Beam bunches in an RF linac.

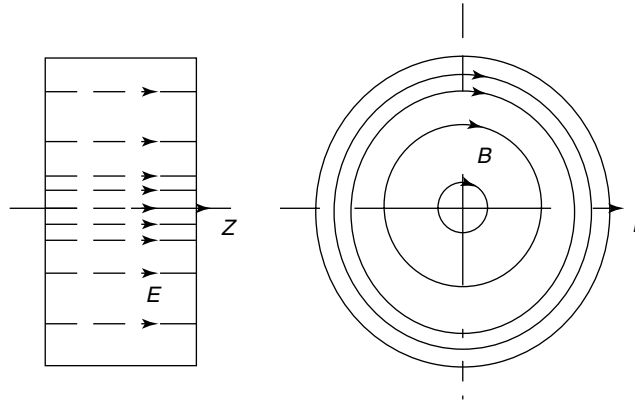


Figure 1.4 Electric (E) and magnetic (B) fields for the transverse-magnetic resonant mode in a cylindrical cavity.

mode is characterized by a longitudinal electric field on axis, which is ideal for acceleration of a charged-particle beam. An important practical consideration is how to construct an efficient linac using these cavities. There have been several solutions. First, an array of independent cavities can be used, each driven by its own RF generator, and each phased independently to provide acceleration along the entire length. This solution is used for superconducting linacs, where its main advantage is operational flexibility.

Another solution is to launch an electromagnetic traveling wave in a long structure consisting of many electromagnetically coupled cells. The traveling-wave structure was used for the 50-GeV electron linac at the SLAC. Although the simplest accelerating structure might appear to be a uniform cylindrical waveguide, it cannot provide continuous acceleration of electrons, because the phase velocity of an electromagnetic wave in a uniform waveguide always exceeds the velocity of light, so that synchronism with the beam is not possible. A structure with modified geometry is required to lower the phase velocity to that of the beam. At SLAC, the linac structure consists of a cylindrical waveguide that contains a periodic array of conducting disks with axial holes, as shown in Fig. 1.5. Each individual cell within a pair of disks is essentially identical to the basic cavity of Fig. 1.4, and the whole structure is equivalent to an array of coupled cylindrical cavities. It can be shown that for this structure the phase velocity can be reduced below the speed of light, as required for particle acceleration. The electrical characteristics of the disk-loaded waveguide structure will be described in more detail in Chapter 3.

The other common method of producing acceleration in a linac is to excite a standing wave in a multicell or coupled-cavity array. Several types of multicell structures have been invented for optimum application over specific ranges of beam velocity. One type of structure is the Alvarez DTL, discussed earlier and shown in Fig. 1.6, which is used to accelerate protons and other ions in the

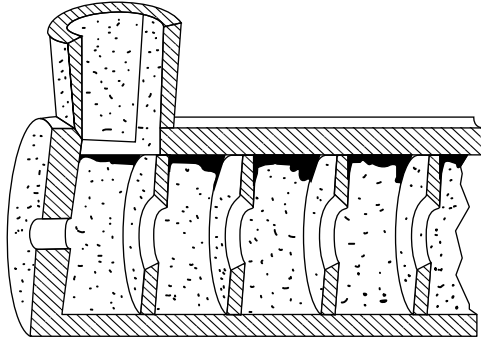


Figure 1.5 The disk-loaded traveling-wave structure, also showing the input waveguide through which the electromagnetic wave is injected into the structure at the end cell. The beam propagates along the central axis and is accelerated by the electric field of the traveling wave.

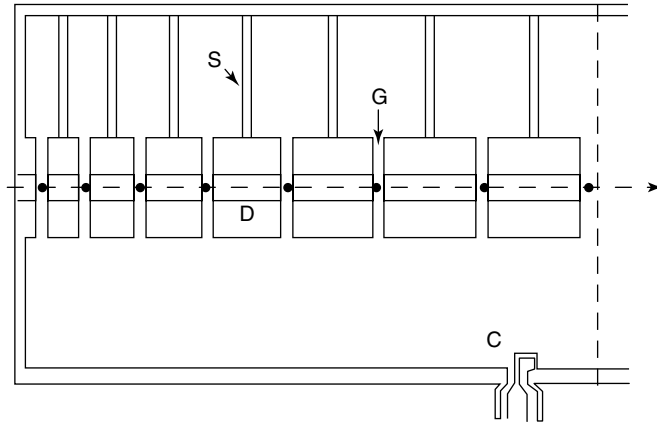


Figure 1.6 Alvarez drift-tube linac structure the drift tubes, when the field has the wrong used for acceleration of medium-velocity polarity for acceleration. The drift tubes D ions. The beam particles are bunched before are supported by the stems S. The cavity is injection into the drift-tube linac. The beam excited by the RF current flowing on a bunches being accelerated in the gaps G a coaxial line into the loop coupler C. shown. They are shielded from the field by

velocity range from about 0.04 to about 0.4 times the speed of light. Unlike the Wideröe structure, in the DTL the fields in adjacent gaps are in phase, and the spacing of the accelerating gaps is nominally equal to the distance the beam travels in one RF period. The DTL structure is not used for electrons, because electrons are so light that their velocity is already above the applicable velocity region at injection from the dc electron gun. Other coupled-cavity linac structures are used for both electrons and protons in the velocity range above about 0.4 times the speed of light. This velocity corresponds to kinetic energies near 50 keV for electrons, the typical injection energy from an electron gun, and near 100 MeV for protons. For example, a coupled-cavity structure called the side-coupled linac (SCL) is used at the Los Alamos Neutron Science Center

(LANSCE) linac at Los Alamos to accelerate the proton beam from 100 to 800 MeV. The transverse-focusing requirements are provided by magnetic-quadrupole lenses mounted within the drift tubes of the DTL, and between structures in a coupled-cavity linac.

The newest accelerating structure for the very-low-velocity range from about 0.01 to 0.06 times the velocity of light is the (RFQ), shown in Fig. 1.7. An electric-quadrupole mode is excited in a cavity resonator loaded with four conducting rods or vanes, placed symmetrically about the beam axis. The RFQ electric field provides strong transverse electric focusing, which is an important requirement for low-velocity protons and heavy ions. Acceleration in the RFQ is obtained by machining a longitudinal-modulation pattern on these four elements to create an array of effective accelerating cells and a longitudinal accelerating field. The RFQ bunches and captures a dc beam injected from the ion source, and then accelerates the beam to high-enough energies for injection into the DTL. The overall result is a significant increase in the focusing strength at low velocities, which enables acceleration of higher-current beams in linacs.

In pulsed linacs, one must distinguish between micropulses and macropulses. We will see later that, within each RF cycle, the longitudinal electric field produces a stable region (the bucket) for the beam. Consequently, the linac fields form a sequence of stable RF buckets separated by one RF period. Each bucket may contain a stable bunch of particles called a *micropulse*.

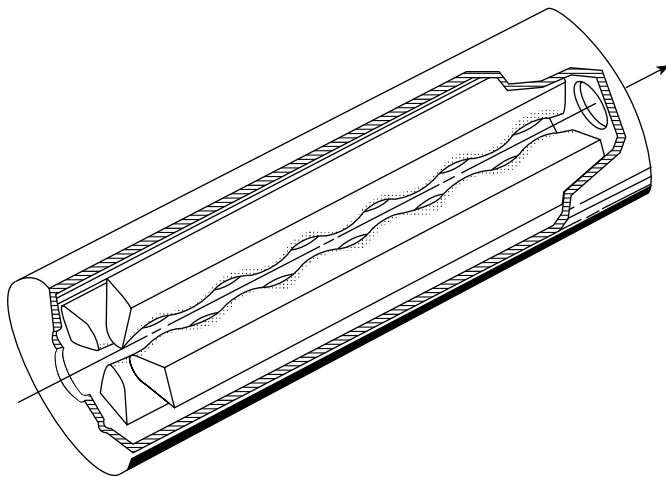


Figure 1.7 The radio-frequency quadrupole (RFQ), used for acceleration of low-velocity ions, consists of four vanes mounted within a cylindrical cavity. The cavity is excited in an electric-quadrupole mode in which the RF electric field is concentrated near the vane tips to produce a transverse RF electric-restoring force for particles that are off-axis. The modulation of the vane tips produces a longitudinal electric-field component that accelerates the beam along the axis.

When the RF generator itself is pulsed, with a period that is generally very long compared with the RF period, the generator pulses are called *macropulses*. The linac may be operated continuously, which is called *continuous-wave* operation. The choice to operate pulsed or continuously depends on several issues. One important issue is the total RF efficiency. If the accelerated beam current is small, most of the power in CW operation is not delivered to the beam, but is dissipated in the structure walls. Instead, if the accelerator is operated pulsed, and the current per RF bucket is increased while maintaining the same average beam current, then a larger fractional power is delivered to the beam, and the efficiency is improved. Another important advantage for pulsed operation is that the peak surface electric field attainable is generally larger for shorter pulses. Thus, if high accelerating fields are required, pulsed operation may be preferred. The main advantage for either longer pulse or CW operation is to reduce the space-charge forces or other beam-current-dependent effects associated with acceleration of beam with high average currents. These effects can be reduced by spreading the total beam charge over more RF buckets, as is done in longer pulse or CW operation.

Because the linac is a single-pass device, the linac length and the ohmic power consumption in the cavity walls may be large compared with circular accelerators, which use the same accelerating cavities over and over. To shorten the accelerator for a given energy gain, it is necessary to raise the longitudinal electric field, but this increases the power dissipation and increases the risk of RF electric breakdown. For high-duty-factor operation, the average power density from RF losses on the cavity walls can produce challenging cooling requirements for the conventional copper-cavity technology. Another approach to these problems that has become increasingly successful in recent years is the use of superconducting niobium cavities.

1.3

Linac Beam Dynamics

Multicell ion linacs are designed to produce a given velocity gain per cell. Particles with the correct initial velocity will gain the right amount of energy to maintain synchronism with the field. For a field amplitude above a certain threshold, there will be two phases for which the velocity gain is equal to the design value, one earlier and the other later than the crest, as shown in Fig. 1.8.

The earlier phase is called the *synchronous phase* and is the stable operating point. It is a stable point because nearby particles that arrive earlier than the synchronous phase experience a smaller accelerating field, and particles that arrive later will experience a larger field. This provides a mechanism that keeps the nearby particles oscillating about the stable phase, and therefore provides phase focusing or phase stability. The particle with the correct velocity at exactly the stable phase is called the *synchronous particle*, and it maintains exact synchronism with the accelerating fields. As the particles approach relativistic

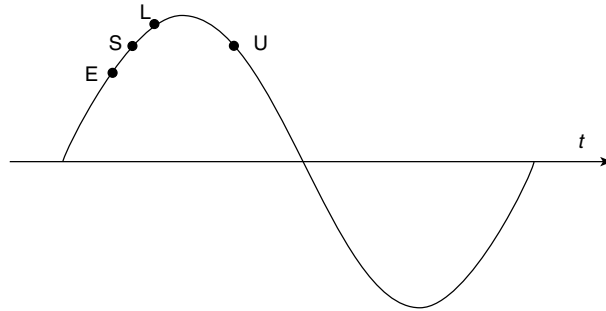


Figure 1.8 Stable (S) and unstable (U) phases, early (E), and late (L) phases.

velocities, the phase oscillations slow down, and the particles maintain a nearly constant phase relative to the traveling wave. After beam injection into electron linacs, the velocities approach the speed of light so rapidly that hardly any phase oscillations take place. With the electromagnetic wave traveling at the speed of light, electrons initially slip relative to the wave and rapidly approach a final phase, which is maintained all the way to high energy. The final energy of each electron with a fixed phase depends on the accelerating field and the value of the phase. In contrast, the final energy of an ion that undergoes phase oscillations about a synchronous particle is approximately determined not by the field, but by the geometry of the structure, which is tailored to produce a specific final synchronous energy. For an ion linac built from an array of short independent cavities, each capable of operating over a wide velocity range, the final energy depends on the field and the phasing of the cavities, and can be changed by changing the field, as in an electron linac.

Longitudinal focusing, obtained by injecting the beam on the leading edge of the wave, is essential for nonrelativistic beams of high intensity. However, RF transverse electric fields also act on the beam as shown by the radial field lines near the edges of the gap in Fig. 1.9, and except for some special cases, the particles that are focused longitudinally experience transverse defocusing forces. Furthermore, additional defocusing effects arise because the injected

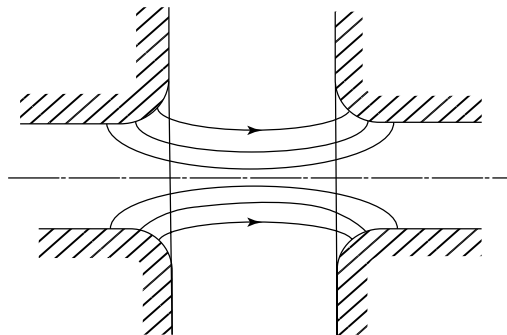


Figure 1.9 Electric-field lines in an accelerating gap.

beam particles always have finite transverse velocities, and the beam particles also exert mutually repulsive Coulomb forces. Thus, provision for transverse focusing must be provided. The most successful solutions for transverse focusing have been either to include separate magnetic-quadrupole focusing lenses or to invent accelerating structures that can provide focusing from the RF transverse electric fields, such as the RFQ.

1.4 Multiparticle Effects

Some applications require beams of high quality that occupy a small volume of phase space, called the *emittance*. Small beam phase volume is necessary if a small output focal spot or small output energy spread is required. As the beam intensity increases, several effects begin to increase the phase volume occupied by the beam, and these may eventually lead to loss of the beam. The most serious intensity limitation in ion linacs is caused by the repulsive space-charge forces, which are usually the most important at lower velocities, where the beam density is highest. The repulsive space-charge forces cause additional defocusing, and because these forces are nonlinear, they distort the particle distribution. Space-charge forces can also produce an extended halo of large-amplitude particles surrounding the main core of the beam. The halo particles can strike the walls and contribute to beam loss that causes radioactivity along the accelerating structure. The radioactivity increases the difficulty of providing routine maintenance of the linac, and thereby reduces the overall operational availability of the linac. For applications requiring high average beam current, control of the halo and beam losses through strong focusing, adequate aperture radius, and proper matching of the beam distribution to the focusing system becomes an important design requirement.

For relativistic electron linacs, the electric (space charge) and magnetic self-fields from the beam tend to cancel, nearly eliminating the total effective space-charge effect. But, short bunches of relativistic particles produce a highly Lorentz-compressed field distribution, and these fields from the beam interact with conducting-boundary discontinuities, producing scattered radiation, called *wakefields*, that act on trailing charges in both the same and later bunches. The wakefields can also increase the beam emittance. Wakefield effects can be reduced by damping the higher-order modes that are the major contributors and reducing discontinuities whenever possible. Certain cavity modes, called *deflecting modes*, can be excited by an off-axis beam, and are the most dangerous. These modes can cause further deflection of trailing particles and under certain conditions lead to an instability known as the *beam-breakup instability*, which results in loss of the beam.

Finally, beam loading occurs, as the beam itself excites the accelerating mode in the cavities. The beam-induced field adds vectorially to the contribution from the generator to produce a modified amplitude and phase. From another

viewpoint, energy is transferred from the beam to each cavity, which unless otherwise corrected, reduces the cavity field and may shift the phase. Beam-loading compensation methods are used successfully to maintain the correct amplitudes and phases in the presence of the beam. Solutions for controlling all these high-intensity effects can significantly influence the design choices for the main accelerator parameters, including frequency, aperture radius, focusing characteristics, cavity tuning, and RF system operation.

1.5 Applications of Modern RF Linacs

For electron linacs, applications of recent interest include (1) electron-positron colliders for elementary-particle-physics research, (2) high-quality electron beams for free-electron lasers, (3) pulsed neutron sources for nuclear physics and material sciences, and (4) X-ray sources for radiotherapy. Electron-positron linear colliders are preferred over circular colliders because synchrotron radiation losses, experienced by relativistic electrons in circular accelerators, are avoided. Furthermore, because of the strong focusing in a linac, high beam quality is achieved, which is required for high luminosity and a high collision rate. Design studies, and research and development for linear colliders in the tetraelectron volt range, are being carried out within the framework of an international collaboration [12]. The most successful commercial application of RF accelerators is the small 10–20-MeV electron linacs for cancer therapy. A few thousand electron linacs are used worldwide for medical irradiations, and this number is growing. Small electron linacs are also used for industrial radiography and radiation processing, including radiation sterilization.

For proton linacs, modern applications include (1) injectors to high-energy synchrotrons for elementary-particle-physics research; (2) high-energy linacs for CW spallation neutron sources used for condensed matter and materials research, production of nuclear fuel, transmutation of nuclear wastes, and accelerator-driven fission-reactor concepts; (3) CW neutron sources for materials irradiation studies related to fusion reactors; and (4) low-energy neutron sources for medical applications such as boron–neutron capture therapy. Design studies for large proton linacs have been carried out for the Accelerator Production of Tritium (APT) project [13] and the neutron spallation source projects in Europe, the European Spallation Source (ESS) [14] and in the United States, where the Spallation Neutron Source (SNS) was recently constructed [15]. There are also linac applications for heavy ions, including (1) linacs for nuclear physics research, (2) ion implantation for semiconductor fabrication, and (3) multigigaelectron volt linacs for heavy-ion-driven inertial-confinement fusion. The most recently commissioned heavy-ion linac is the lead-ion linac at CERN [16].

A recent worldwide compendium of existing and planned scientific linacs [17] listed 174 linacs distributed over the Americas, Europe, and Asia.

Historically, two significant large linac projects are the SLC electron–positron linear collider at SLAC, shown in Fig. 1.10, and the LANSCE linac at Los Alamos, shown in Fig. 1.11. The main parameters of these two linacs are summarized in Table 1.1. The SLC at SLAC is the first linear collider, built to produce the Z^0 vector boson near a center-of-mass energy of 91 GeV. It used the 2-mile SLAC electron linac, which was built in the 1960s [18]. Positrons were produced by bombarding a target with a 30-GeV e^- beam. More details of this unique facility are summarized elsewhere [19].

The LANSCE linac,[21] formerly known as *LAMPF*, began operation in the early 1970s as a pion factory for research in nuclear and high-energy physics. It delivers the highest average proton beam power of any existing accelerator. It can deliver 1-mA, 800-MeV proton beams to a fixed target, or an H beam for multiturn injection into the proton storage ring, where the accumulated beam is extracted in short pulses for neutron scattering research.

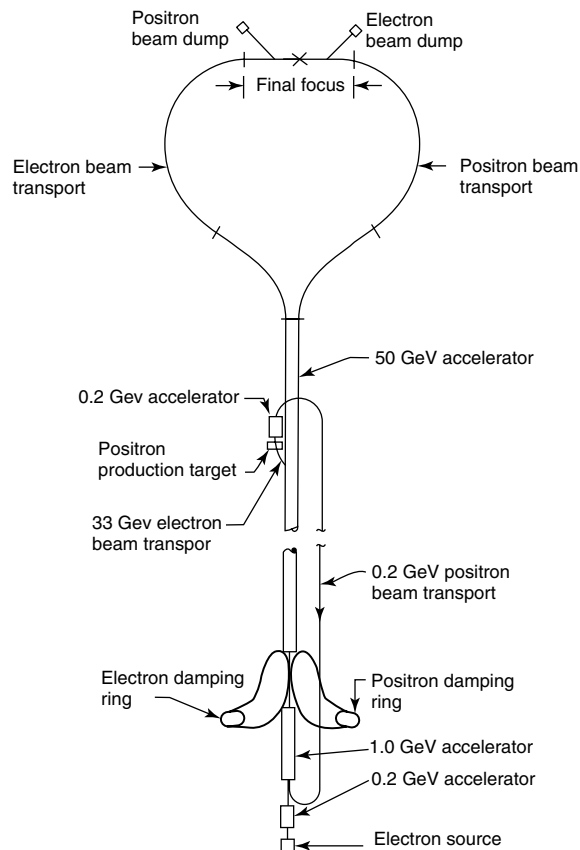
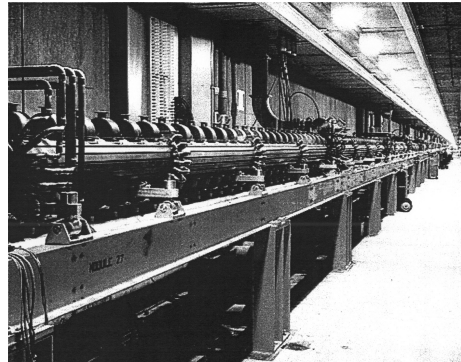


Figure 1.10 The SLAC linear collider.



(a)

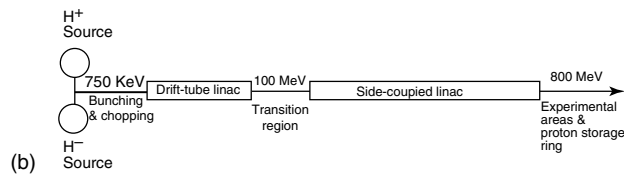


Figure 1.11 The 800-MeV LANSCE proton linac.

Table 1.1 Parameters of SLC and LANSCE linacs [20].

Facility	SLC at SLAC	LANSCE at Los Alamos (H ⁻ data)
Application	e ⁻ /e ⁺ collider for high-energy physics research	Linac for high-intensity beams of H ⁻ and H ⁺
First beam	1967	1972
Species	Electrons and positrons	H ⁺ and H ⁻
Beam intensity	2–3.5 × 10 ¹⁰ particles per pulse	11 mA peak H ⁻ (average over 825 μs macropulse)
Beam pulse	120 Hz, 0.06–3 μs	120 Hz, 825 μs
Output energy	46.6 GeV	800 MeV
Accelerating structure data	960 3-m structures for traveling-wave acceleration at 2856 MHz; 60–130 MW peak power, 25 kW average power	201.25-MHz DTL from 0.75 to 100 MeV
Length	3000 m	805-MHz SCL from 100 to 800 MeV 62-m DTL, 731-m SCL

1.6 Accelerator-Physics Units, Unit Conversions, and Physical Constants

In this book we will use the SI or MKS units, with two notable exceptions. The magnetic flux density will sometimes be expressed in gauss. The conversion

factor between the SI unit tesla and gauss is 1 Gauss = 10^{-4} tesla. Beam-particle energy will be given in electron volts or eV units, rather than joules. The electron volt is defined as the energy acquired by a particle with charge equal to the electron charge that has been accelerated through a potential difference of 1 V. The conversion factor between electron volts and joules is approximately $1.602 \times 10^{-19} = 1 \text{ eV}$. Finally, instead of the particle mass, we will usually give the rest energy, mc^2 in megaelectron volt units. Some frequently used physical constants are given in Table 1.2 [22].

1.7 Useful Relativistic Mechanics Relationships

We assume that the reader has a basic knowledge of classical and relativistic mechanics. In this section we present a brief review of basic formulas from relativistic mechanics that will be useful. Consider a particle of mass m and speed v . If c is the speed of light, it is customary to define a normalized velocity β as $\beta = v/c$, and a relativistic mass factor γ , defined as $\gamma = 1/\sqrt{1 - \beta^2}$. Some other important definitions include the relativistic momentum of a particle, $\mathbf{p} = \gamma m \mathbf{v}$, the kinetic energy, $W = (\gamma - 1)mc^2$, the rest energy, mc^2 , and the total energy, $U = W + mc^2 = \gamma mc^2$. The nonrelativistic limit applies when $\beta \ll 1$. It is often convenient to convert between velocity, energy, and momentum, and the following relationships are helpful. The conversion from velocity β to kinetic energy W is

$$\gamma = 1/\sqrt{1 - \beta^2}, W = (\gamma - 1)mc^2 \quad (1.1)$$

The inverse conversion is

$$\gamma = (W + mc^2)/mc^2, \beta = \sqrt{1 - 1/\gamma^2} \quad (1.2)$$

The following relationships between small differences are sometimes useful: $\delta\gamma = \gamma^3\beta\delta\beta$, $\delta\gamma = \beta\delta(\beta\gamma)$, $\delta W = mc^2\delta\gamma$, $\delta p = mc\delta(\beta\gamma)$. Particle dynamics

Table 1.2 Physical constants.

Speed of light	c	$2.99792458 \times 10^8 \text{ m/s}$
Elementary charge	e	$1.60217733 \times 10^{-19} \text{ C}$
Electron mass	m_e	$0.51099906 \text{ MeV}/c^2$
Proton mass	m_p	$938.27231 \text{ MeV}/c^2$
Atomic mass unit ^a	m_u	$931.49432 \text{ MeV}/c^2$
Permeability of free space	μ_0	$4\pi \times 10^{-7} \text{ T}\cdot\text{m/A}$
Permittivity of free space	ϵ_0	$1/\mu_0 c^2 = 8.854187817 \dots \times 10^{-12} \text{ F/m}$
DC resistivity of copper (293 K)	$1/\sigma$	$1.7 \times 10^{-8} \text{ }\Omega\cdot\text{m (nominal)}$

^aMass of (^{12}C)/12.

is obtained from Newton's law relating the force and the rate of change of momentum:

$$\mathbf{F} = \frac{d\mathbf{p}}{dt} = m \frac{d(\gamma \mathbf{v})}{dt} \quad (1.3)$$

For a particle of charge q in an electromagnetic field, the Lorentz force on particle with charge q and velocity \mathbf{v} in an electric field \mathbf{E} and a magnetic field \mathbf{B} , is given by

$$\mathbf{F} = q(\mathbf{E} + \mathbf{v} \times \mathbf{B}) \quad (1.4)$$

1.8 Maxwell's Equations

The laws describing all classical electromagnetic phenomena are known as *Maxwell's equations*. These equations relate the electric and magnetic fields, and the charge and current sources. Maxwell's four equations in vacuum (where $\mathbf{D} = \epsilon_0 \mathbf{E}$ and $\mathbf{B} = \mu_0 \mathbf{H}$), expressed in differential form, are as follows:

$$\nabla \cdot \mathbf{E} = \rho / \epsilon_0, \text{ Gauss's law} \quad (1.5)$$

$$\nabla \cdot \mathbf{B} = 0 \quad (1.6)$$

$$\nabla \times \mathbf{E} = -\partial \mathbf{B} / \partial t, \text{ Faraday's law} \quad (1.7)$$

$$\nabla \times \mathbf{B} = \mu_0 \mathbf{J} + \mu_0 \epsilon_0 \partial \mathbf{E} / \partial t, \text{ Ampère's law} \quad (1.8)$$

where ρ is the charge density and \mathbf{J} is the current density. A charge-continuity equation $\nabla \cdot \mathbf{J} = -\partial \rho / \partial t$ is derived from these equations. Maxwell's equations can also be expressed in what is often a more convenient integral form:

$$\int \mathbf{E} \cdot d\mathbf{S} = \frac{1}{\epsilon_0} \int \rho dV, \text{ Gauss's law} \quad (1.9)$$

$$\int \mathbf{B} \cdot d\mathbf{S} = 0 \quad (1.10)$$

$$\oint \mathbf{E} \cdot d\mathbf{l} = - \int \frac{\partial \mathbf{B}}{\partial t} \cdot d\mathbf{S}, \text{ Faradays law} \quad (1.11)$$

$$\oint \mathbf{B} \cdot d\mathbf{l} = \mu_0 \int \left(\mathbf{J} + \epsilon_0 \frac{\partial \mathbf{E}}{\partial t} \right) \cdot d\mathbf{S}, \text{ Ampère's law} \quad (1.12)$$

It can be shown that the electric and magnetic fields can propagate as electromagnetic waves. When the charges and currents are zero, the wave equations in Cartesian coordinates are as follows:

$$\nabla^2 \mathbf{E} - \frac{1}{c^2} \frac{\partial^2 \mathbf{E}}{\partial t^2} = 0; \quad \nabla^2 \mathbf{B} - \frac{1}{c^2} \frac{\partial^2 \mathbf{B}}{\partial t^2} = 0 \quad (1.13)$$

where $c = 1/\sqrt{\mu_0 \epsilon_0}$ is the speed of light in vacuum.

Maxwell's equations are composed of four coupled first-order partial differential equations. Two of the equations, Eqs. (1.6) and (1.7), have no charge or current source terms, and may be called the *homogeneous equations*. The other two equations, Eqs. (1.5) and (1.8), do contain source terms and may be called the *inhomogeneous equations*. Although in principle the four equations may be solved for any given problem, it is often convenient to solve a problem using potentials from which the fields may be derived. It is common to define the scalar potential ϕ , and the vector potential \mathbf{A} , which are functions of space and time, such that

$$\mathbf{B} = \nabla \times \mathbf{A}, \quad \mathbf{E} = -\nabla\phi - \frac{\partial \mathbf{A}}{\partial t} \quad (1.14)$$

With these definitions it can be shown [23] that the two homogeneous equations are automatically satisfied. The potentials are not uniquely specified from Eq. (1.14), and uncoupled source equations may be obtained by substituting Eq. (1.14) into Eqs. (1.5) to (1.8), and by imposing what is called the *Lorentz condition*, [24]

$$\nabla \cdot \mathbf{A} + \frac{1}{c^2} \frac{\partial \phi}{\partial t} = 0 \quad (1.15)$$

The resulting equations for the potentials have the symmetric, decoupled form of inhomogeneous wave equations [25]

$$\nabla^2 \phi - \frac{1}{c^2} \frac{\partial^2 \phi}{\partial t^2} = -\rho/\epsilon_0 \quad (1.16)$$

and

$$\nabla^2 \mathbf{A} - \frac{1}{c^2} \frac{\partial^2 \mathbf{A}}{\partial t^2} = -\mu_0 \mathbf{J} \quad (1.17)$$

In the course of some of our discussions on RF cavities, we will consider the solution of Eqs. (1.15) to (1.17) within a closed region of space containing no free charges, surrounded by an equipotential surface. In this case Eq. (1.6) can be satisfied by choosing $\phi = 0$ [26]. Then, from Eq. (1.15) we have

$$\nabla \cdot \mathbf{A} = 0 \quad (1.18)$$

and Eq. (1.14) reduces to [27]

$$\mathbf{B} = \nabla \times \mathbf{A}, \quad \mathbf{E} = -\frac{\partial \mathbf{A}}{\partial t} \quad (1.19)$$

For this case, the electric and magnetic fields are obtained from the vector potential alone, which must satisfy Eqs. (1.17) and (1.18).

1.9 Conducting Walls

The boundary conditions at the interface between vacuum and an ideal perfect conductor can be derived by applying the integral forms of Maxwell's equations to small pillbox-shaped volumes at the interface. One finds that only the normal electric-field component and the tangential magnetic-field component can be nonzero just outside the conductor surface. If \hat{n} is a vector normal to the interface, Σ is the surface charge density on the conductor, and \mathbf{K} is the surface-current density, the boundary conditions that must be satisfied by the fields just outside the conductor are

$$\begin{aligned}\hat{n} \cdot \mathbf{E} &= \Sigma / \epsilon_0 \\ \hat{n} \times \mathbf{H} &= \mathbf{K} \\ \hat{n} \cdot \mathbf{B} &= 0 \\ \hat{n} \times \mathbf{E} &= 0\end{aligned}\tag{1.20}$$

No perfect conductors exist, but certain metals are very good conductors. Copper, with a room-temperature resistivity of $\rho = 1/\sigma = 1.7 \times 10^{-8} \Omega\text{-m}$, is the most commonly used metal for accelerator applications. For a good but not perfect conductor, fields and currents are not exactly zero inside the conductor, but are confined to within a small finite layer at the surface, called the *skin depth*. In a real conductor, the electric and magnetic fields, and the current decay exponentially with distance from the surface of the conductor, a phenomenon known as the *skin effect*. The skin depth is given by

$$\delta = \sqrt{\frac{2}{\sigma \mu_0 \omega}}\tag{1.21}$$

Because of the skin effect, the ac and dc resistances are not equal. It is convenient to define the ac or RF surface resistance $R_s = 1/\sigma \delta$, and using Eq. (1.21), we find $R_s = \sqrt{\mu_0 \omega / 2\sigma}$, which shows that the ac surface resistance is proportional to the square root of the frequency. If dS is the area element on the cavity walls, the average power dissipation per cycle is

$$P = \frac{R_s}{2} \int H^2 dS\tag{1.22}$$

Physically, the skin effect is explained by the fact that RF electric and magnetic fields applied at the surface of a conductor induce a current, which shields the interior of the conductor from those fields. For frequencies in the 100 MHz range and for a good conductor like copper, the skin depth δ is of the order 10^{-6} m, and R_s is in the milliohm range. The use of superconducting materials dramatically reduces the surface resistance. For the RF surface

resistance of superconducting niobium, we will use an approximate formula

$$R_s(\Omega) = 9 \times 10^{-5} \frac{f^2(\text{GHz})}{T(^{\circ}\text{K})} \exp\left[-\alpha \frac{T_c}{T}\right] + R_{\text{res}} \quad (1.23)$$

where $\alpha = 1.83$, and $T_c = 9.2$ K is the critical temperature. R_{res} is known as the *residual resistance*; it is determined by imperfections in the surface, and typically is approximately 10^{-9} to 10^{-8} Ω . The superconducting surface resistance is roughly 10^{-5} lower than that of copper.

1.10 Group Velocity and Energy Velocity

Linac technology requires the propagation of electromagnetic waves in transmission lines, waveguides, and cavities. There are no truly monochromatic waves in nature. A real wave exists in the form of a wave group, which consists of a superposition of waves of different frequencies and wave numbers. If the spread in the phase velocities of the individual waves is small, the envelope of the wave pattern will tend to maintain its shape as it moves with a velocity that is called the *group velocity*. The simplest example of a wave group, shown in Fig. 1.12, consists of two equal-amplitude waves, propagating in the $+z$ direction, with frequencies ω_1 and ω_2 , and wave numbers k_1 and k_2 , which we can express in complex exponential form as

$$\begin{aligned} V(z, t) &= e^{j(\omega_1 t - k_1 z)} + e^{j(\omega_2 t - k_2 z)} \\ &= 2 \cos\left[\frac{(\omega_1 - \omega_2)t - (k_1 - k_2)z}{2}\right] e^{j[(\omega_1 + \omega_2)t - (k_1 + k_2)z]/2} \end{aligned} \quad (1.24)$$

The exponential factor describes a traveling wave with the mean frequency and mean wave number, and the first factor represents a slowly varying

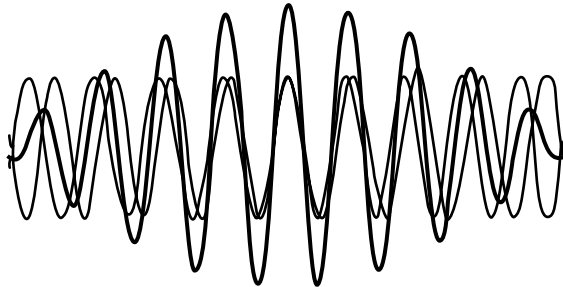


Figure 1.12 Wave composed of two components with different frequencies and wave numbers.

modulation of the wave amplitude. The phase velocities of component waves are ω_1/k_1 and ω_2/k_2 , and the mean phase velocity is

$$v_p = \frac{\omega_1 + \omega_2}{k_1 + k_2} = \frac{\bar{\omega}}{\bar{k}} \quad (1.25)$$

The group velocity is defined as the velocity of the amplitude-modulation envelope, which is

$$v_g = \frac{\omega_1 - \omega_2}{k_1 - k_2} \rightarrow \frac{d\omega}{dk} \quad (1.26)$$

Generally, the mean phase velocity and the group velocity are not necessarily equal; they are equal when there is a linear relation between frequency and wave number, as for the ideal transmission line. The waveguide dispersion curve is a plot of ω versus k . Figure 1.13 shows an example of a dispersion curve for a uniform waveguide. The phase velocity at any point on the curve is the slope of the line from the origin to that point, and the group velocity is the slope of the dispersion curve, or tangent at that point. For the uniform guide, one finds $v_p v_g = c^2$, where $v_g < c$ and $v_p > c$.

A more general example of wave group is the wave packet, which describes a spatially localized wave group, as shown in Fig. 1.14. Again, the group velocity, rather than the phase velocity, must be used to characterize the motion of a wave packet. For example, the transient filling of a waveguide with

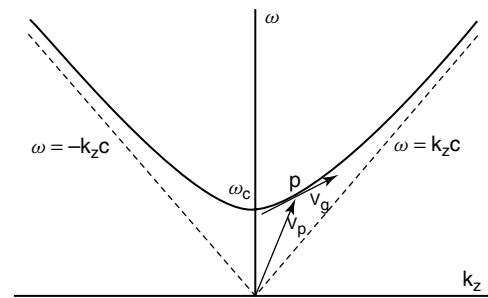


Figure 1.13 Example of dispersion curve for uniform waveguide, $\omega^2 = \omega_c^2 + (k_z c)^2$, showing graphically the meaning of phase and group velocity at the point p on the curve. The group velocity at point p is the tangent to the curve at that point. The phase velocity is the slope of the line from the origin to the point p .

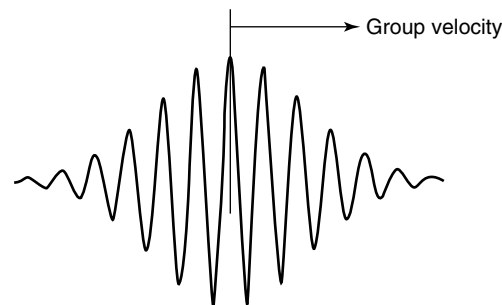


Figure 1.14 Wave packet.

electromagnetic energy must be described in terms of the motion of a wave packet, which will have a leading edge that moves at approximately the group velocity for practical cases where dispersion is not too large. The phase velocity does not appear in the description, because it describes the speed of individual waves that make up the wave packet, rather than the wave packet itself, which really consists of an interference pattern of these waves.

The energy velocity is defined as the velocity of electromagnetic energy flow, which, for a traveling wave moving in the $+z$ direction, is

$$v_E = \frac{P_+}{U_\ell} \quad (1.27)$$

where P_+ is the wave power, the electromagnetic energy per unit time crossing a transverse plane at fixed z , and U_ℓ is the stored electromagnetic energy per unit length. For cases of practical interest, the energy velocity is equal to the group velocity [28]. This result is useful for evaluating the energy velocity because the group velocity at the operating point is easy to determine from the slope of the dispersion curve.

1.11

Coaxial Resonator

Some accelerating cavities, especially for relatively low frequencies below about 100 MHz, are variants of the simple coaxial resonator. Without worrying now about the specific modifications needed to produce a practical accelerating cavity, we consider the properties of a coaxial resonator. A coaxial resonator, shown in Fig. 1.15, is formed by placing conducting end walls on a section of coaxial line formed by an inner conductor of radius a and an outer conductor with radius b . When the enclosed length is an integer multiple of half wavelengths, transverse electromagnetic (TEM) resonant standing-wave modes exist, where both the electric and magnetic fields have only transverse components. Resonance occurs when the boundary condition on the end walls, $E_r = 0$, is satisfied. This condition occurs when the conducting walls are separated by a distance $\ell = p\lambda/2$, $p = 1, 2, 3, \dots$. To obtain the solution, first imagine a current wave on the inner conductor traveling in the $+z$ direction, $I_0 e^{j(\omega t - kz)}$. From the integral form of Ampere's law, the current produces an azimuthal magnetic field given by $B_\theta = I_0 e^{j(\omega t - kz)} \mu_0 / 2\pi r$. Given the magnetic field, the radial electric field can be obtained from the differential form of Faraday's law as $E_r = I_0 e^{j(\omega t - kz)} \mu_0 c / 2\pi r$. Likewise, we find that a wave traveling in the $-z$ direction has components $I_0 e^{j(\omega t + kz)}$, $B_\theta = I_0 e^{j(\omega t + kz)} \mu_0 / 2\pi r$, and $E_r = -I_0 e^{j(\omega t + kz)} \mu_0 c / 2\pi r$. Adding these two waves produces a standing wave satisfying the boundary condition that the tangential electric field E_r vanishes on the end walls at $z = 0$ and ℓ . The nonzero field components are

$$B_\theta = \frac{\mu_0 I_0}{\pi r} \cos(p\pi z / \ell) \exp[j\omega t] \quad (1.28)$$

$$E_r = -2j\sqrt{\frac{\mu_0}{\varepsilon_0}} \frac{I_0}{2\pi r} \sin(p\pi z/\ell) \exp[j\omega t] \quad (1.29)$$

where $\omega = k_z c = \frac{p\pi c}{\ell}$, $p = 1, 2, 3, \dots$. We note that the complex j factor in Eq. (1.29) denotes a 90° phase shift in time between the left and right sides of the equation, which can be obtained explicitly by substituting the identity $j = e^{j\pi/2}$. The electromagnetic stored energy is

$$U = \frac{\mu_0 \ell I_0^2 \ln(b/a)}{2\pi} \quad (1.30)$$

and the quality factor or Q , including the losses on the end walls, is

$$Q_0 = \frac{p\pi}{R_s} \sqrt{\frac{\mu_0}{\varepsilon_0}} \frac{\ln(b/a)}{\left[\ell \left(\frac{1}{a} + \frac{1}{b} \right) + 4 \ln \frac{b}{a} \right]} \quad (1.31)$$

The lowest mode corresponds to $p = 1$, the half-wave resonator. Figure 1.15 shows the peak current and voltage distributions for $p = 1$, where the voltage is $V = \int_a^b E_r dr$. The cavity in Fig. 1.15 could be modified to make it suitable for acceleration by introducing beam holes in the inner and outer conductors at $z = \ell/2$ where the voltage is maximum. The beam, moving along a radial path, will see no field when it is within the inner conductor, and can see an accelerating field in the region on both sides between the inner and outer conductors. The injection phase could be chosen so that the beam travels across the inner conductor while the field reverses sign, so that the beam can be accelerated on both the entrance and exit sides of the inner conductor. The conductor radii could be chosen so that the beam receives the maximum energy gain on each side.

Another widely used type of resonator for accelerator applications is the coaxial line terminated at one end by a short and at the other end by a capacitance, as shown in Fig. 1.16. The capacitive termination can be

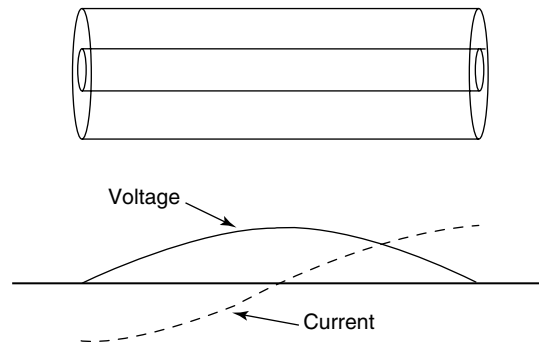


Figure 1.15 Coaxial resonator with voltage and current standing waves for $p = 1$.

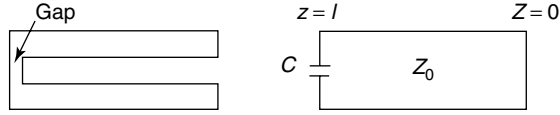


Figure 1.16 Coaxial resonator.

accomplished in practice with a coaxial line that has a gap at one end between the center conductor and the conducting end wall. An electric field suitable for acceleration may exist between the inner conductor and either the end wall or the cylindrical wall. Thus, beam holes can be introduced near the gap, allowing either a radial or an axial trajectory. Resonant modes correspond approximately to the length λ equal to an odd multiple of a quarter wavelength, the lowest mode being a quarter-wave resonator. Design formulas for the quarter-wave resonator, including the contribution to the capacitance from fringe fields, are given by Moreno [29].

1.12

Transverse-Magnetic Mode of a Circular Cylindrical Cavity

Most cavity resonators used in electron and proton linacs are derived from the simple cylindrical or pillbox cavity. Fortunately, an analytic solution exists for the fields in a pillbox cavity. Beginning with a cylinder of radius R_c , we place conducting end plates at the axial coordinates $z = 0$ and ℓ . In the pillbox cavity, the holes on the end plates that must be provided for the beam are ignored. We assume a simple azimuthally symmetric trial solution of the form $E_z(r, z, t) = R(r)e^{j\omega t}$. This solution must satisfy the wave equation with the condition that E_z vanishes at the cylindrical boundary, $r = R_c$, where it is tangential. The wave equation in cylindrical coordinates is

$$\frac{\partial^2 E_z}{\partial z^2} + \frac{1}{r} \frac{\partial E_z}{\partial r} + \frac{\partial^2 E_z}{\partial r^2} - \frac{1}{c^2} \frac{\partial^2 E_z}{\partial t^2} = 0 \quad (1.32)$$

Substituting the trial solution into Eq. (1.32), we obtain a differential equation for the radial function $R(r)$, which is the well-known Bessel's equation of order zero. The magnetic field is obtained from Ampère's law from Section 1.8. The nonzero field components of the complete solution are given by

$$\begin{aligned} E_z &= E_0 J_0(k_r r) \cos(\omega t) \\ B_\theta &= -\frac{E_0}{c} J_1(k_r r) \sin(\omega t) \end{aligned} \quad (1.33)$$

The radial field distributions are shown graphically in Figures 1.4 and 1.17. To satisfy the boundary condition, the resonant frequency of this mode must be $\omega_c = k_r c = 2.405c/R_c$, which is independent of the cavity length. The mode

is called a *transverse-magnetic mode* because the z component of the magnetic field is zero, and in the conventional nomenclature the mode is called a TM_{010} mode for reasons that will be explained shortly. The total electromagnetic stored energy can be calculated from the peak electric stored energy, and the result is

$$U = \frac{\pi \varepsilon_0 \ell R_c^2}{2} E_0^2 J_1^2(2.405) \quad (1.34)$$

The average power dissipated on the cylindrical walls and the end walls is

$$P = \pi R_c R_s E_0^2 \left(\frac{\varepsilon_0}{\mu_0} \right) J_1^2(2.405) (\ell + R_c) \quad (1.35)$$

The quality factor is

$$Q = \frac{\omega_c U}{P} = \frac{2.405 \sqrt{\mu_0 / \varepsilon_0}}{2R_s} \frac{1}{1 + R_c / \ell} \quad (1.36)$$

The electric field is maximum at $r = 0$, where J_0 is maximum. Two useful values of J_1 are the maximum value, which is $J_1(1.841) = 0.5819$, and the value of J_1 at the cylindrical wall, which is $J_1(2.405) = 0.5191$. The magnetic field is maximum at $k_r R = 0.5819$, where $J_1(k_r R)$ is maximum. Therefore, $B_{\max} / E_{\max} = 0.5819 / c = 19.4 \text{ G/MV/m}$.

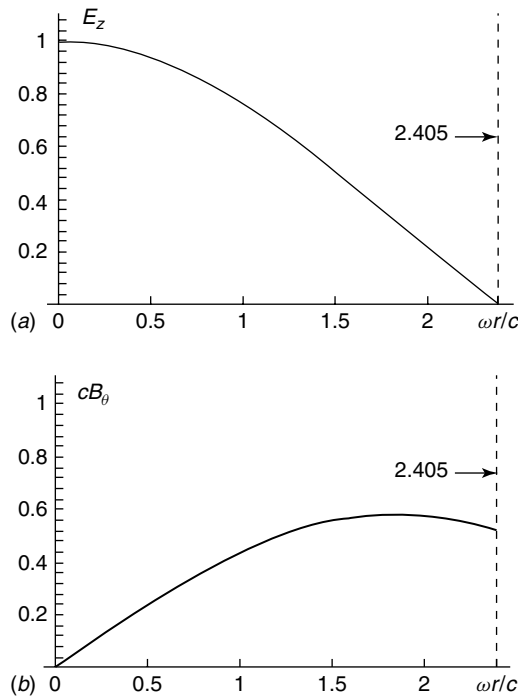


Figure 1.17 Fields for a TM_{010} mode of a cylindrical (pillbox) cavity resonator.

1.13 Cylindrical Resonator Transverse-Magnetic Modes

There are other transverse-magnetic modes with the same radial Bessel-function solution, corresponding to fitting a half-integer number of guide wavelengths within the length ℓ . We label the different longitudinal modes with the index p , and adopt the conventional nomenclature TM_{01p} , $p = 1, 2, 3, \dots$. The dispersion relation is the same as for a uniform waveguide, except that the longitudinal wave number is restricted to those discrete values required to satisfy the boundary conditions at the two ends. The modes lie on the curve given by $\omega^2/c^2 = k_r^2 + k_z^2$, where $k_r = 2.405/R_c$ and $k_z = 2\pi/\lambda_g = \pi p/\ell$. Then, the dispersion relation becomes a discrete spectrum of points that are sprinkled on a hyperbolic curve, as shown in Fig. 1.18. The TM_{010} mode, discussed in Section 1.12, is the lowest mode with $p = 0$. The dispersion relation gives the resonant frequency of this mode as the cutoff frequency $\omega_c = k_r c = 2.405c/R_c$.

There exist additional transverse-magnetic modes of a cylindrical cavity, corresponding to different radial and azimuthal solutions. The general expressions for the field components are as follows:

$$\begin{aligned}
 E_z &= E_0 J_m(k_{mn}r) \cos m\theta \cos(p\pi z/\ell) \exp[j\omega t] \\
 E_r &= -\frac{p\pi}{\ell} \frac{a}{x_{mn}} E_0 J'_m(k_{mn}r) \cos m\theta \sin(p\pi z/\ell) \exp[j\omega t] \\
 E_\theta &= -\frac{p\pi}{\ell} \frac{ma^2}{x_{mn}^2 r} E_0 J_m(k_{mn}r) \sin m\theta \sin(p\pi z/\ell) \exp[j\omega t] \\
 B_z &= 0 \\
 B_r &= -j\omega \frac{ma^2}{x_{mn}^2 r c^2} E_0 J_m(k_{mn}r) \sin m\theta \cos(p\pi z/\ell) \exp[j\omega t] \\
 B_\theta &= -j\omega \frac{a}{x_{mn} c^2} E_0 J'_m(k_{mn}r) \cos m\theta \cos(p\pi z/\ell) \exp[j\omega t] \quad (1.37)
 \end{aligned}$$

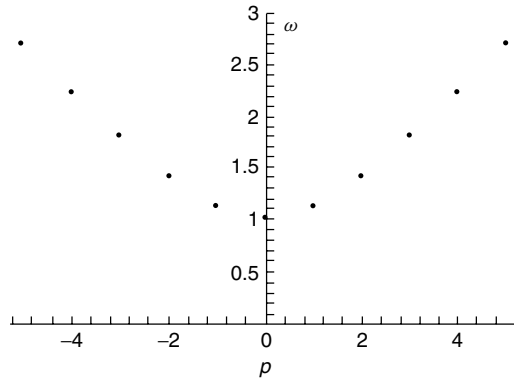


Figure 1.18 Dispersion curve for the TM_{01p} family of modes of a circular cylindrical cavity.

The general dispersion relation is $\omega^2/c^2 = k_{mn}^2 + k_z^2$, where $k_{mn} = x_{mn}/R_c$ and $k_z = 2\pi/\lambda_{guide} = p\pi/\ell$, $p = 0, 1, 2, \dots$. Some values of the zeros of the Bessel functions, x_{mn} , are given in Table 1.3. The nomenclature of the TM_{mnp} modes is defined as follows. The subscript m ($m = 0, 1, 2, \dots$) is the number of full period variations in θ of the field components. The subscript n ($n = 1, 2, 3, \dots$) is the number of zeros of the axial field component in the radial direction in the range $0 < r \leq R_c$, excluding $r = 0$. The subscript p ($p = 0, 1, 2, \dots$) is the number of half period variations in z of the fields.

1.14 Cylindrical Resonator Transverse Electric Modes

Similarly, there exist additional transverse electric modes of a cylindrical cavity, corresponding to solutions with the zero axial component of the electric field. The general field-component expressions for the transverse electric modes are as follows:

$$\begin{aligned}
 B_z &= B_0 J_m(k_{mn}r) \cos m\theta \sin(p\pi z/\ell) \exp[j\omega t] \\
 B_r &= \frac{p\pi}{\ell} \frac{a}{x'_{mn}} B_0 J'_m(k_{mn}r) \cos m\theta \cos(p\pi z/\ell) \exp[j\omega t] \\
 B_\theta &= -\frac{p\pi}{\ell} \frac{ma^2}{x'_{mn}{}^2 r} B_0 J_m(k_{mn}r) \sin m\theta \cos(p\pi z/\ell) \exp[j\omega t] \\
 E_z &= 0 \\
 E_r &= j\omega \frac{ma^2}{x'_{mn}{}^2 r} B_0 J_m(k_{mn}r) \sin m\theta \sin(p\pi z/\ell) \exp[j\omega t] \\
 E_\theta &= j\omega \frac{a}{x'_{mn}} B_0 J'_m(k_{mn}r) \cos m\theta \sin(p\pi z/\ell) \exp[j\omega t] \quad (1.38)
 \end{aligned}$$

The general dispersion relation is $\omega^2/c^2 = k_{mn}^2 + k_z^2$, where $k_{mn} = x'_{mn}/R_c$ and $k_z = 2\pi/\lambda_{guide} = p\pi/\ell$, $p = 0, 1, 2, \dots$. The x'_{mn} are the zeros of the derivatives of the Bessel functions and are given in Table 1.4. The nomenclature of the TE_{mnp} modes is defined as follows. The subscript m ($m = 0, 1, 2, \dots$) is the number of full period variations in θ of the field components. The subscript n ($n = 1, 2, 3, \dots$) is the number of zeros of the axial field component in

Table 1.3 Zeros of $J_m(x)$ or x_{mn} .

m	x_{m1}	x_{m2}	x_{m3}
0	2.405	5.520	8.654
1	3.832	7.016	10.173
2	5.136	8.417	11.620

Table 1.4 Zeros of J'_m or x'_{mn} .

m	x'_{m_1}	x'_{m_2}	x'_{m_3}
0	3.832	7.016	10.174
1	1.841	5.331	8.536
2	3.054	6.706	9.970

the radial direction in the range $0 < r \leq R_c$, excluding $r = 0$. The subscript p ($p = 0, 1, 2, \dots$) is the number of half period variations in z of the fields.

Problems

- 1.1. What is the kinetic energy in units of both joules and electron volts for an electron accelerated through a dc potential of 1 MV?
- 1.2. Find an expression for the fractional error when the nonrelativistic approximation for kinetic energy as a function of β is used. (a) At what values of β and γ does the error in kinetic energy equal 1%? (b) To what kinetic energy does this correspond, for electrons and for protons?
- 1.3. If the only nonzero components of the electromagnetic field in cylindrical coordinates are E_r , E_z , and B_θ , write the nonzero components of the Lorentz force for a particle of mass m and charge q moving along the z direction with velocity v .
- 1.4. The rate of work done by a force \mathbf{F} acting on a particle with velocity \mathbf{v} is $\mathbf{F} \cdot \mathbf{v}$. Using the definition of the Lorentz force and the appropriate vector relationship, derive the expression for the rate of kinetic energy gain for a particle of charge q , and show that the magnetic force does not contribute.
- 1.5. A cylindrical resonator has a diameter of 1.5 in. (3.81 cm) and length ℓ of 1 in. (2.54 cm). (a) Calculate the resonant frequency of the TM_{010} , TM_{110} , TE_{011} , TE_{111} , and TE_{211} modes, and list in order of increasing frequency. (b) For the two lowest-frequency modes, plot the dispersion relation, $f(= \omega/2\pi)$ versus $k_z(=p\pi/\ell)$, both on the same graph. For simplicity, label the abscissa with the longitudinal mode index p (i.e., units of π/ℓ for $p = 0$ to $p = 5$). (Recall that the TE modes have no resonance at $p = 0$.)
- 1.6. Repeat the exercise of Problem 1.5 for the same diameter resonator but with different lengths. (a) $\ell = 7.725$ cm. Note the frequency of the TE_{112} mode compared to the TM_{010} mode. How did it change relative to the result of Problem 1.5? (b) $\ell = 25.4$ cm. Note that all of the first five TE_{11p} modes now lie below the TM_{010} frequency.
- 1.7. Calculate the RF surface resistance and skin depth of room-temperature copper at 400 MHz. Use a dc resistivity $\sigma^{-1} = 1.7 \times 10^{-8} \Omega\text{-m}$.

- 1.8. Calculate the RF surface resistance of superconducting niobium at 400 MHz. Assume a residual resistance $R_{\text{residual}} = 100 \times 10^{-9} \Omega$. What is the ratio of the RF surface resistance of superconducting niobium to that of room-temperature copper? (a) Assume $T = 4.2$ K; (b) assume $T = 2.0$ K.
- 1.9. Design a room-temperature cylindrical cavity that operates in the TM_{010} mode at 400 MHz with an axial electric field $E_0 = 1$ MV/m, and a length $\ell = \lambda/2$, where λ is the RF wavelength in free space. (a) Calculate the length and diameter of the cavity. (b) Calculate the maximum B and H fields on the cavity wall. Where does this occur? (c) Calculate the B and H fields on the cylindrical wall. (d) Calculate the electromagnetic stored energy in the cavity. (e) Use the value of R_s from Problem 1.7 for a room-temperature copper surface to calculate the power loss P , the quality factor Q_0 , and the decay time τ . (f) Repeat part (e) using R_s from Problem 1.8 for a 4.2-K niobium surface.
- 1.10. Design a half-wave coaxial cavity to be used as a 100-kW resonant load at 400 MHz. To absorb the RF power, use a 20-cm-diameter stainless steel pipe as the center conductor inside a 60-cm-diameter copper cylinder with copper end walls. This type of cavity is easily cooled by flowing water through the center conductor. (a) Ignoring any effects of the coupling loop and probe, calculate the length of the cavity. (b) Assume that the room-temperature surface resistance of stainless steel is 6.5 times that of copper. (From Problem 1.7 the copper surface resistance at 400 MHz is 0.0052Ω .) Calculate the power dissipated on the center conductor, end walls, and outer wall. (c) Calculate the cavity stored energy and the unloaded Q . (d) What is the peak power density in watts per square centimeter on the inner and outer conductors?
- 1.11. A 25-MHz quarter-wave coaxial-cavity resonator with characteristic impedance 50Ω is designed as a buncher for heavy-ion beams. (a) If the impedance at the open end of the cavity (where the electric field is maximum) could really be made infinite, what would be the length of the inner conductor? (b) If we want to reduce the size by restricting the length of the inner conductor to $\ell = 1$ m, what lumped capacitance would be required at the open end?
- 1.12. Accelerator cavities require ports through the cavity walls, not only for RF drive and RF pickup probes, but also for the beam and for vacuum pumping. Cylindrical pipes are commonly used, and such pipes will support waveguide modes. Consider a cylindrical cavity operating in a TM_{010} mode with beam pipes connected at the center of each end wall. Assume each beam pipe has the same inner radius b , which is much less than the cavity radius. (a) Why do you expect the fields from the cavity to attenuate in the pipes? (b) Show that if the cavity excites a TM_{01} waveguide mode in the beam pipes at a frequency well below cutoff, the wave power and the E and B fields attenuate with distance x along the pipe according to the approximate formula $\text{dB} = -20.9x/b$. Note

that it is convenient to describe the attenuation of a wave with power P and field E in decibels, or dB, where $\text{dB} = 10 \log_{10} P/P_0 = 20 \log_{10} E/E_0$, where P_0 and E_0 are the input reference values. (c) The TE_{11} mode has the lowest cutoff frequency of the modes in a cylindrical pipe, and below the cutoff frequency the attenuation will be the slowest. If this mode is excited in the pipe, show that at a frequency well below cutoff, the attenuation is described by the approximate formula $\text{dB} = -16.0x/b$. (d) Assuming a pipe with radius $b = 0.5$ inches that is excited in a TE_{10} mode by the cavity, calculate the total attenuation in decibels if the pipe length is 2 in. Also express the answer as the fractional attenuation of the field. (e) The attenuation in a waveguide below cutoff frequency was derived ignoring ohmic losses. What do you think has happened to the energy in the wave?

References

- 1 The betatron and the related induction linac accelerate beams using nonharmonic time-dependent fields. These machines produce pulsed electric fields by induction from a magnetic pulse in accordance with Faraday's law. The orbit of the betatron is circular, and that of the induction linac is straight.
- 2 Ising G., (1924) *Ark. Mat. Fys.* **18**, (No. 30), 1–4.
- 3 Wideröe R., (1928) *Arch. Electrotech.* **21**, 387.
- 4 (1994) For a discussion of this and other work by Wideröe, see P. Waloschek, *The Infancy of Particle Accelerators—Life and Work of Rolf Wideröe*, DESY 94–039, Deutsches Elektronen-Synchrotron, Notkestrasse 85–22603, Hamburg, March.
- 5 Lawrence E.O. and Edlefsen N.E., (1930) *Science* **72**, 376.
- 6 Sloan D.H. and Lawrence E.O., (1931) *Phys. Rev.* **38**, 2021.
- 7 Sloan D.H. and Coate W.M., (1934) *Phys. Rev.* **46**, 539.
- 8 Alvarez L.W., (1946) *Phys. Rev.* **70**, 799.
- 9 Alvarez L.W., Bradner H., Franck J.V., Gordon H., Gow J.D., Marshall L.C., Oppenheimer F., Panofsky W.K.H., Richmond C., and Woodward J.R., (1955) *Rev. Sci. Instr.* **26**, 111, and (1955); *Rev. Sci. Instr.* **26**, 210.
- 10 Hansen W.W., Kyhl R.L., Neal R.B., Panofsky W.K.H., Chodorow M., and Ginzton E.L., (1955) *Rev. Sci. Instrum.* **26**, 134.
- 11 For a more complete early history of linacs, see Blewett J.P., in *Linear Accelerators*, Lapostolle P.M., and Septier A.L., North Holland Publishing, 1970 pp. 1–16.
- 12 For an overview of the issues and of some very interesting advanced electron-linac concepts for linear-collider applications, see *International Linear Collider Technical Review Committee Report*, prepared for the Interlaboratory Collaboration for R&D Towards TeV-scale Electron-Positron Linear Colliders, Committee Chairman, G. A. Loew (SLAC), December, 1995; see also *Design Issues of TeV Linear Colliders*, CERN/PS 96–30 (LP), 1996 European Part. Accel. Conf., ed. J. P. Delahaye (CERN).
- 13 Lawrence G.P., *et al.*, (1996) *Conventional and Superconducting RF Linac Designs for the APT Project*, Proc. 1996 Int. Linac Conf., Geneva, August 26–30.
- 14 *Outline Design of the European Spallation Neutron Source*, ed. Gardner I.S.K., Lengeler H., and Rees, G.H., ESS 95–30-M, September, 1995.
- 15 Holtkamp, N., *Status of the SNS Linac: an Overview*, Proc. of EPAC 2006, Edinburgh, Scotland, June 26–30, pp. 29–33.

- 16 Haseroth H.R., *The Lead Ion Injector at CERN*, Proc. 1996 Int. Linac Conf., Geneva, August 26–30, 1996.
- 17 *Compendium of Scientific Linacs*, Provisional Edition, 18th Int. Co., CERN-PS Division, Geneva, August, 26–30, 1996.
- 18 *The Stanford Two-Mile Accelerator*, Neal R.B., Benjamin W.A., New York, (1968); Panofsky W.K.H., *The Creation of SLAC Leading to 30 Years of Operation*, Proc. 18th Int. Linear Accel. Conf., August, 26–30, 1996, Geneva, ed. Hill C. and Vretenar M., CERN 96–07, Geneva, November 15, 1996 p. 3.
- 19 *SLC Design Handbook*, Erickson R., Stanford 1984; also Seeman J., (1991) *Ann. Rev. Nucl. Part. Sci.* **41**, 3891; also Seeman J.T., *Advances of Accelerator Physics and Technologies*, Advanced Series on Directions in High Energy Physics, Vol. 12, Schopper H., 1993 p. 219.
- 20 Erickson R.E.O., Hughes V.W., and Nagel D.E., *The Meson Factories*, University of California Press, Los Angeles, 1991; also Livingston M.S., *LAMPF, A Nuclear Research Facility*, LA-6878-MS, September 1977; also Livingston M.S., *Origins and History of the Los Alamos Meson Physics Facility*, LA-5000.
- 21 *Compendium of Superconducting Linacs*, Provisional Edition, 18th Int. Linac Conf. Geneva, August, 26–30, 1996.
- 22 (1987) *Rev. Mod. Phys.* **57**, 1121.
- 23 Jackson J.D., 1975 *Classical Electrodynamics*, 2nd ed., John Wiley & Sons, New York, pp. 219–223.
- 24 Potentials that satisfy Eq. (11) are said to belong to the Lorentz gauge.
- 25 The beauty of this result has been previously noted. See Feynman R.P., Leighton R.B., and Sands M., *The Feynman Lectures on Physics*, Addison Wesley, 1963 Vol. 2, p. 18–11.
- 26 See Condon E.U., (1940) *J. App. Phys.* **11**, 502; Condon E.U., (1941) *J. App. Phys.* **12**, 129.
- 27 Potentials that satisfy Eq. (14) are said to belong to the Coulomb gauge. Note that for this case, because $\phi = 0$, Eq. (11) is also satisfied and the potentials belong simultaneously to the Lorentz and Coulomb gauges.
- 28 Watkins D.A., 1958 *Topics in Electromagnetic Theory*, John Wiley & Sons, New York, pp. 12–14; Bevensee R.M., 1964 *Electromagnetic Slow Wave Systems*, John Wiley & Sons, New York, pp. 17–19.
- 29 Moreno T., 1948 *Microwave Transmission Design Data*, Dover, New York, pp. 227–230.